Sensors and Actuators B 260 (2018) 877–887

Contents lists available at ScienceDirect

Sensors and Actuators B: Chemical

journal homepage: www.elsevier.com/locate/snb

H_2S sensing characteristics of Ni-doped $CaCu_3Ti_4O_{12}$ films synthesized by a sol-gel method

Arisara Boontum[a], Ditsayut Phokharatkul[b], Jose H. Hodak[a,c,d], Anurat Wisitsoraat[b,e], Satreerat K. Hodak[a,*]

[a] Department of Physics, Faculty of Science, Chulalongkorn University, Bangkok, 10330, Thailand
[b] Carbon-based Devices and Nanoelectronics Laboratory, Pathumthani, 12120, Thailand
[c] Universidad de Buenos Aires, Facultad de Ciencias Exactas y Naturales, Departamento de Química Inorgánica, Analítica y Química Física, Pabellón 2, Ciudad Universitaria, C1428EHA, Buenos Aires, Argentina
[d] CONICET – Universidad de Buenos Aires, Instituto de Química-Física de Materiales, Ambientes y Energía (INQUIMAE), Buenos Aires, Argentina
[e] Department of Common and Graduate Studies, Sirindhorn International Institute of Technology, Thammasat University, Pathumthani, Thailand

ARTICLE INFO

Article history:
Received 18 September 2017
Received in revised form
23 December 2017
Accepted 6 January 2018
Available online 6 January 2018

Keywords:
Calcium copper titanate
Ni doping
Hydrogen sulfide
Semiconducting gas sensor
Sol-gel method

ABSTRACT

The problem of detecting the toxic hydrogen sulfide (H_2S) gas at part per million levels in air by means of simple solid state gas sensors is relevant to environmental and gas processing industries. In this work, high-performance H_2S gas sensors are developed based on nickel-doped calcium copper titanate (Ni-doped CCTO) thin films synthesized by a sol-gel method. From gas-sensing measurements, the response of Ni-doped CCTO sensing films increased substantially with increasing Ni doping level from 1.5 to 7.3 wt%, revealing a catalytic effect of Ni on the surface reactions with adsorbed H_2S molecules. In particular, 7.3 wt% Ni-doped CCTO sensors offered a high response of 120 for 10 ppm of H_2S at the optimal operating temperature of 250 °C, an order of magnitude higher than that of undoped one. In addition, the response time dropped significantly from ~80 s to ~4 s while the recovery time slightly improved as the Ni doping content increased from 0 to 7.3 wt%. Moreover, the Ni-doped CCTO sensors exhibited good reproducibility and high H_2S selectivity against ethanol, H_2, NO_2 and NH_3. Therefore, the Ni-doped CCTO sensors are highly promising for sensitive and selective detections of H_2S.

1. Introduction

The task of determining part per million (ppm) levels of the highly toxic hydrogen sulfide gas in the atmosphere is of particular interest for environmental protection in various risky areas such as chemical centers, oil or gas fields and sewage systems. The danger of H_2S depends on its concentration, exposure time and individual condition. For example, the lowest-observed-adverse-effect level (LOAEL) of 1.87 ppm has been reported to induce neurological and cardio-respiratory effects to asthmatic patients [1]. Also, H_2S concentrations of 250 ppm can lead to a rapid loss of consciousness followed by lethal effects [2] while extended exposure to lower concentrations may cause difficulties in respiration, irritation of the eyes and throat, drowsiness and headache to healthy people [3]. Although H_2S can be perceived even at low concentrations by its characteristic rotten egg odor, the sense of smell to this gas will fail after an extended exposure period and high H_2S concentrations will lead to the sudden loss of ability to sense this smell. For workers in an industrial environment, a threshold limit value of H_2S is recommended to be 10 ppm [4]. The monitoring of H_2S may be achieved by means of chromatographic, electrochemical, infrared and semiconductor gas detectors. Among these, the sensors based on chemiresistive metal oxide semiconductor sensors excel in simplicity, small dimensions and cost efficiency, making them particularly attractive for portable monitoring and hand-held medical diagnostic equipment. Despite the advantages of metal oxide semiconductor sensors, they generally suffer from poor selectivity, reproducibility and long-term stability and there are continuous efforts to improve their performances. Nanostructured and thin film forms of metal oxides have been widely studied as the active mediums of chemiresistive gas-sensing devices. Sev-

* Corresponding author at: Department of Physics, Faculty of Science, Chulalongkorn University, Bangkok, 10330, Thailand.
E-mail address: satreerat.h@chula.ac.th (S.K. Hodak).

https://doi.org/10.1016/j.snb.2018.01.090
0925-4005/

eral nanomaterials have shown high sensitivity towards H_2S such as CuO-NiO/ferrite micro/nanoparticles [5,6], WO_3 nanowires [7,8], SnO_2 mesowires and nanoribbons [9,10]. The main drawbacks of these materials are their unstable thermal and electrical properties over extended periods of time and poor reproducibility, which considerably hamper their commercialization. On the other hand, thin films of semiconductor metal oxides are reproducible and stable but generally offer lower sensitivity and selectivity. Compositing and doping of metal oxide films with additives are known as effective approaches to overcome some of these limitations [11,12]. Thus, one of the main efforts in sensor research is to find suitable dopants for metal oxide thin films in order to improve their chemical sensitivity towards a particular gas while retaining high reproducibility and robustness of simple metal oxide thin films. Several metal oxides in pure and doped forms have been extensively explored for gas-sensing applications. Tin, zinc and tungsten oxides (SnO_2, ZnO and WO_3) are among the most well-known gas-sensing materials, which are already being used commercially for detections of various gases due to their low cost, high sensitivity towards reducing or oxidizing gases and ease of microfabrication [13–16]. However, the stability, sensitivity and selectivity of the sensors made with these oxides may be surpassed by other novel material compositions without compromising the simplicity of design and fabrication.

Calcium copper titanate, $CaCu_3Ti_4O_{12}$ (CCTO), which is well-known for its giant dielectric constant, is a relatively new material of choice in the gas sensing field [17–19]. CCTO belongs to the group of pseudo perovskite structures, which has a lattice constant of 7.390 Å and does not undergo any structural phase transitions over the temperature range of 100–600 K [20]. Pure and metal-doped CCTO thin films can be prepared by several methods including reactive RF magnetron sputtering [21], sol-gel methods [18], pulsed laser deposition (PLD) [19] and metal organic chemical vapor deposition (MOCVD) [22]. Among these, the sol-gel deposition is a simple process that uses low cost equipment but can produce homogeneous films on a variety of substrates over large areas. The effects of metal doping in CCTO ceramics on its electrical properties including La [23], Fe [24], Ag [25] and Ni [26] have been explored. However, there are still only few gas-sensing studies of metal-doped CCTO thin films. Recently, Fe-doped CCTO thin films have demonstrated attractive H_2S sensing performances [27]. It is thus compelling to apply other doping elements to improve the gas-sensing characteristics of CCTO. Selecting a suitable metal doping for metal oxide semiconductor gas sensors usually involves an educated guess based on known strong interaction or high catalytic activity towards a target gas of a particular element. Successful examples of this strategy include Ni-doped ZnO nanofibers responsive to C_2H_2 [28], Cu-doped [29] and Fe-doped $LaCo_{1-x}Fe_xO_3$ nanoparticles selective to CO [30], Ni-doped SnO_2 nanowires sensitive to butanol and formaldehyde [31], Ni-doped SnO_2 nanofibers highly sensitive to NO_2 [32] and Pd-doped WO_3 nanoparticles highly selective to H_2 [33]. In the case of H_2S, transition metals including Fe, Ag, Cu and Ni are known to exhibit strong chemical interaction with sulfur-based compounds and high catalytic activity towards desulfurization reactions [34,35]. In particular, several Ni-incorporated materials have been shown to improve H_2S sensing responses of various metal oxide gas sensors [5,31,36,37]. However, these reported H_2S sensors still suffer from relatively poor selectivity [5,36,38] and unsatisfactory H_2S detection limit of larger than 2 ppm [5,36]. In this work, Ni doping is applied with varying Ni contents up to 7.3 wt% to enhance the H_2S sensing characteristics of CCTO thin films prepared via a simple sol-gel method. Specifically, this study focuses on the H_2S response at ppm and sub ppm levels, reproducibility and selectivity for practical H_2S sensing applications.

2. Methods

2.1. Preparation of CCTO films

Ni-doped $CaCu_3Ti_4O_{12}$ (CCTO) thin films were synthesized by a sol-gel method using acetic acid as solvent. The starting materials were calcium acetate hydrate ($Ca(C_2H_3O_2)_2{\cdot}xH_2O$, Sigma, 99%), copper (II) acetate monohydrate ($Cu(II)(C_2H_3O_2){\cdot}H_2O$, Fluka, 99%), titanium (IV) isopropoxide ($Ti(OCH(CH_3)_2)_4$, Sigma, 97%), and nickel oxide (NiO, Merck). Ni doping was done at various concentrations including 0, 1.5, 4.4, and 7.3 wt% (corresponding to 0.0, 3.7, 11.4 and 19.0 mol% of Ni). To obtain a desired Ni doping level, the corresponding molar amount of NiO (0.8, 2.4, and 4.4 milimoles) was first completely dissolved in 25 g of acetic acid at 120 °C. To the obtained nickel acetate solution, 0.855 g of calcium acetate and 2.943 g of copper acetate were added, and the mixture was placed on a magnetic stirrer for 24 h at room temperature. Next, titanium isopropoxide was added with gentle stirring followed by addition of ethylene glycol (3 ml) and formamide (3 ml), and the mixture was placed on a hot plate at 120 °C for 3–5 h until homogeneous sol-gel was obtained. In a typical batch, the amount of titanium isopropoxide used for the preparation of undoped CCTO is 6.130 g (21.6 milimoles). In the synthesis of doped CCTO, the number of NiO moles used for doping was subtracted from the molar amount of titanium isopropoxide. Undoped and Ni-doped CCTO films were cast by spin coating 0.1 ml of the sol-gel precursor on alumina and silicon substrates, which were cut into small pieces of $2.5 \times 2.5\ cm^2$ and $1 \times 1\ cm^2$, respectively.

Prior spin coating, the substrates were cleaned in acetone and isopropanol with the help of an ultrasonic cleaner. For each doping condition, the CCTO precursor sol-gel was coated on the cleaned substrate by spinning at 1500 rpm for 40 s using a spin coater (model P6700 series). The films were then baked at 120 °C for 20 min on a hot plate in order to dry the gel and remove volatile organic compounds. Finally, the films were annealed at 800 °C for 1 h in an oven under air atmosphere. This whole process is referred to a one-layer film deposition, which yields a typical film thickness of ca. 100 nm. The one-layer deposition procedure was repeated four times to obtain the film thickness of ca. 400 nm. Silicon and alumina were used as substrates for different proposes. A set of films was cast on alumina for gas sensor fabrication while another set of films was deposited on silicon substrates for material characterization.

2.2. Film characterization

The crystal structure and phase composition of CCTO films on alumina and silicon substrates were characterized by X-ray diffraction (XRD). The X-ray measurements were done on a diffractometer (Bruker D8 Discover) using $CuK\alpha_1$ ($\lambda = 1.5406$ Å) radiation with 40 kV and 40 mA in the 2θ range of 20° to 80° with a scan step of 0.02°. Field emission scanning electron microscope (FE-SEM) (SU-8000, Hitachi) was used to examine the surface morphology and the cross section of CCTO films deposited on alumina substrates. The oxidation states of each element in the films were determined by X-ray photoelectron spectroscopy (XPS) (Kratos, Axis Ultra DLD). The chemical compositions of Ni-doped films were determined by energy dispersive x-ray spectroscopy (EDX) (EDAX, AMETEK) operated at 10 keV. Raman spectra for the pure and Ni-doped CCTO phases were collected using a Raman spectrometer (NTEGRA, NT-MDT) with a 633 nm laser source.

2.3. Gas sensor fabrication and measurements

A pair of interdigitated gold electrodes was patterned on top of the CCTO films on alumina substrates. The films were first spin

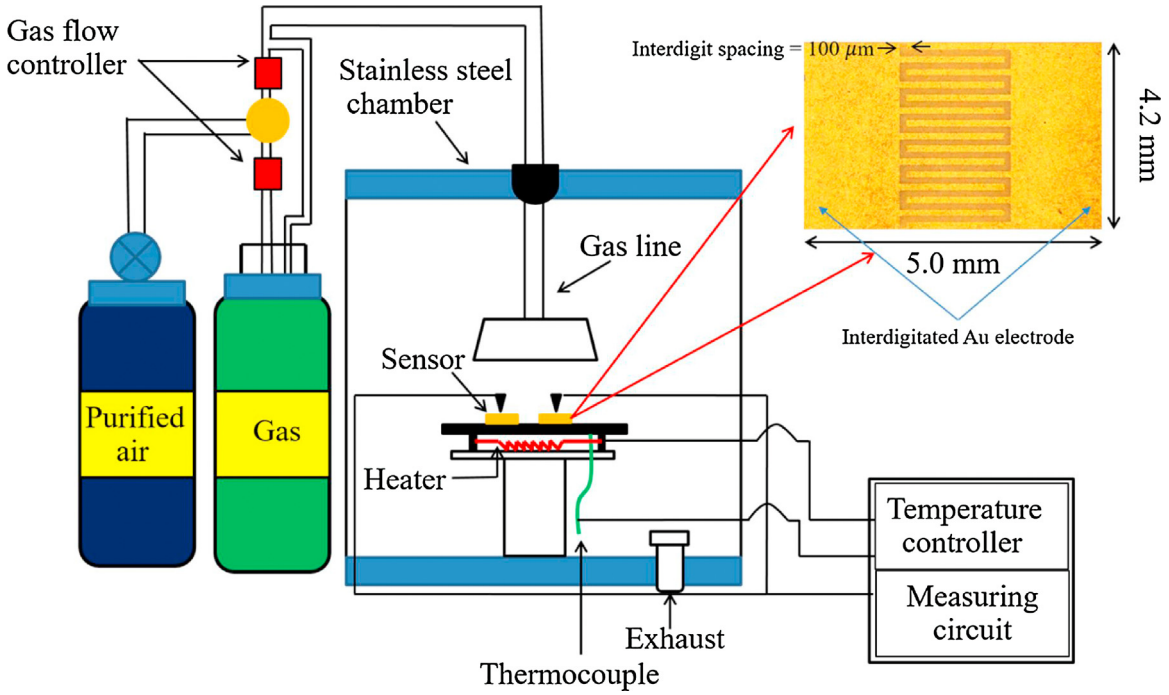

Fig. 1. Schematic diagram of the setup for gas sensing measurements and details of the Ni-doped CCTO sensors. The top view photograph of an actual sensor with its dimensions is shown in the picture on the upper right corner.

coated with a positive photoresist (Shipley S1805) at 3000 rpm for 90 s followed by baking at 90 °C for 60 s to dry the resist and remove volatile organic compounds. The photoresist films were exposed with UV light for 35 s through a mask with interdigitated patterns. The exposed films were removed with developer before baking a second time at 115 °C for 60 s. The 50 nm-thick Cr and 300 nm-thick Au layers were successively sputtered on the developed resist pattern to form the electrodes of the gas sensor devices. Next, the photoresist layer was dissolved in acetone under ultrasonication to lift off excess metal on the photoresist. The sensing devices were finally cut to release individual 4.2 × 5.0 mm sensor chips as shown in Fig. 1.

Before gas-sensing experiments, the sensors were baked at 400 °C in air to remove any remaining organic compounds from the surface of the films. Several individual sensors were probed in a chamber for simultaneous gas-sensing measurements. The sensors were tested towards various gases including NO_2, H_2, NH_3, H_2S and ethanol. The operating temperature was varied in the range of 150–350 °C to determine an optimum operating temperature. The target gas was injected into the chamber and the resistance of the film was measured with a computer controlled system as shown in the diagram of Fig. 1. In addition, the gas sensing properties of the CCTO sensors were characterized in terms of sensor response, response time, recovery time and selectivity as functions of gas concentration and operating temperature. The sensor response was evaluated using the relation, $R = R_a/R_g$, where R_a and R_g are the resistance of the n-type semiconductor sensor measured in dry air atmosphere and reducing tested gases, respectively. In the case of oxidizing gases, the response is the reciprocal to $R_{ox} = R_g/R_a$.

3. Results and discussion

3.1. Characterization of the sensing material

The main physical and chemical properties of Ni-doped CCTO films were first assessed to aid the interpretation of sensor characteristics. Fig. 2(a) shows XRD patterns of Ni-doped CCTO thin films

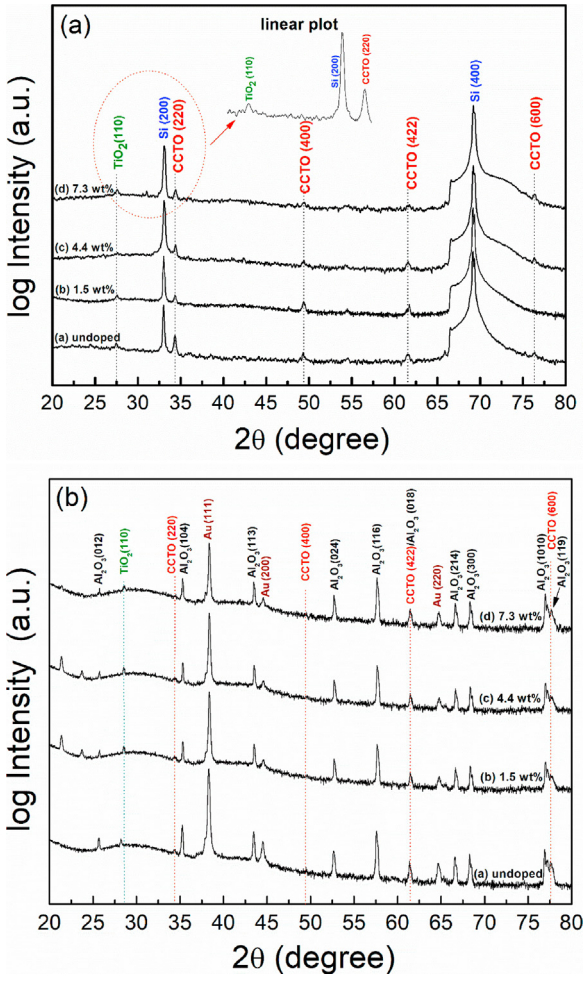

Fig. 2. X-ray diffraction patterns of Ni-doped CCTO films on (a) silicon and (b) alumina substrates.

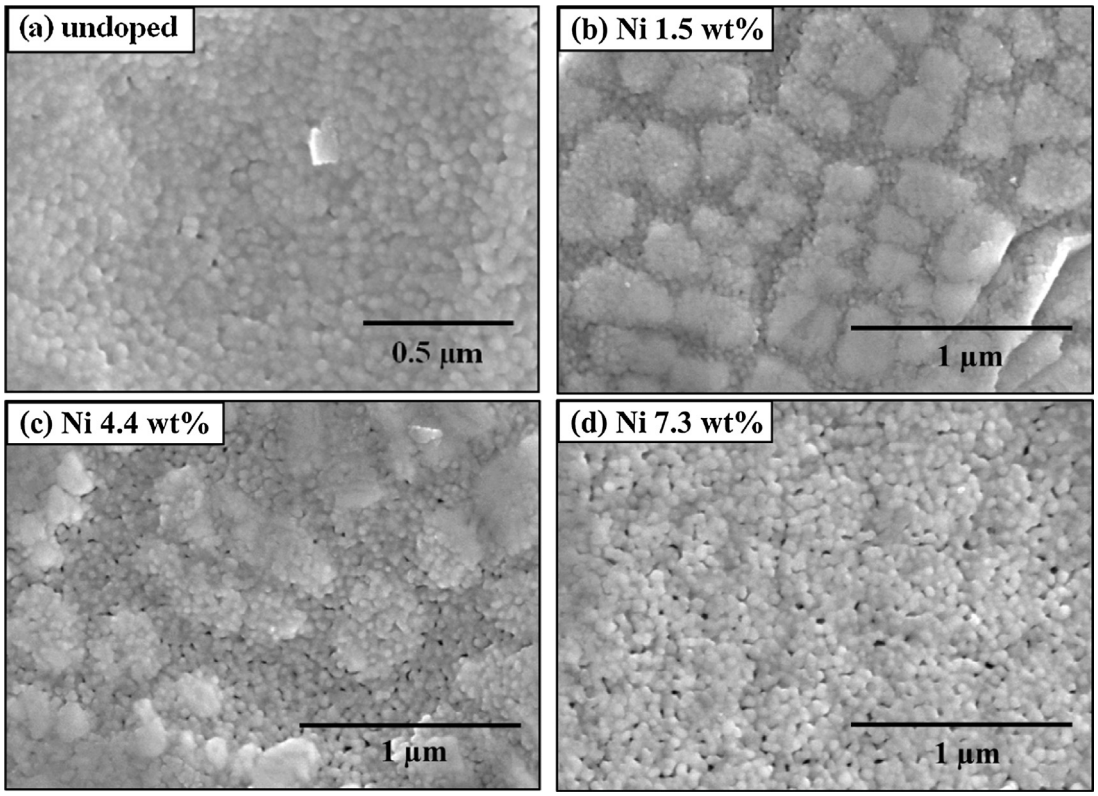

Fig. 3. FESEM images of (a) undoped, (b) 1.5 wt% Ni-doped, (c) 4.4 wt% Ni-doped and (d) 7.3 wt% Ni-doped CCTO films on alumina substrates annealed at a fixed temperature of 800 °C.

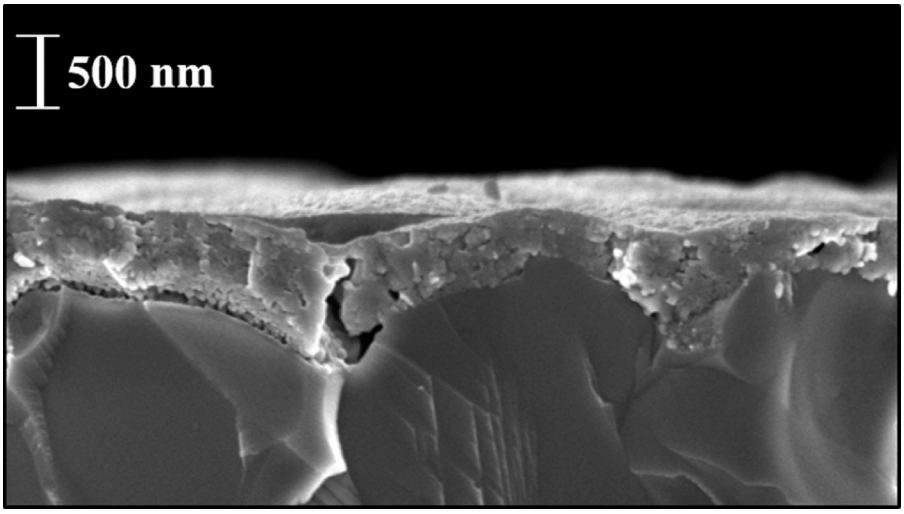

Fig. 4. Typical cross sectional SEM image of 7.3 wt% Ni-doped CCTO thin film on an alumina substrate.

deposited on silicon substrates. Diffraction patterns of all the films similarly display the dominant diffraction peaks of CCTO phase occurring at 2θ values of 34.27°, 49.26° and 61.39°. These signals correspond to the diffraction from (220), (400) and (422) planes of the cubic perovskite structure of CCTO (JCPDS 21-0140), respectively. The lattice constant of CCTO in our thin films was calculated from Bragg's law on (220) plane to be 7.3809 Å. The lattice constant value is slightly lower than that of bulk CCTO (7.391 Å). There is no detectable shift of the diffraction positions of CCTO in the Ni-doped films. The X-ray diffraction data allow us to rule out the formation of $NiTiO_3$, which should show the XRD peak signals on (104), (110), and (116) planes at 2θ values of 32.99°, 35.55° and 53.90°, respectively [39]. In addition to the CCTO signatures, the strong diffraction peaks of (200) and (400) planes from the silicon substrates and small peaks of rutile TiO_2 impurity are also detected.

The crystal structure and phase composition were also examined in the Ni-doped CCTO thin films deposited on alumina substrates equipped with interdigitated electrodes as shown in Fig. 2(b). The diffraction peaks of CCTO agree with those of the Ni-doped CCTO thin films on silicon substrate. The XRD patterns present Au diffraction peaks from the electrodes and the other dominant diffraction features from alumina substrates. The crystal structure as well as the general crystallinity of the films on both types of substrates are not significantly different, demonstrating

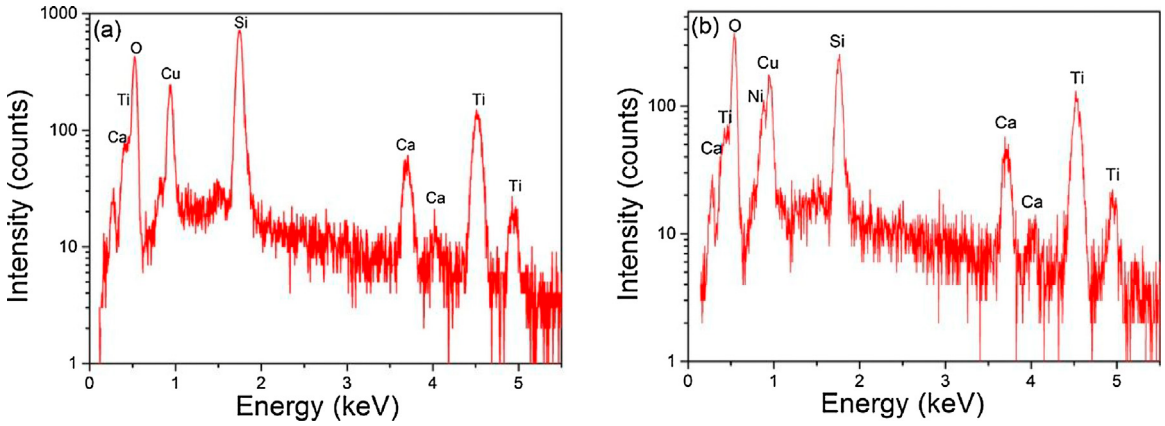

Fig. 5. EDX spectra of (a) 0 wt% Ni-doped CCTO and (b) 7.3 wt% Ni-doped CCTO thin films.

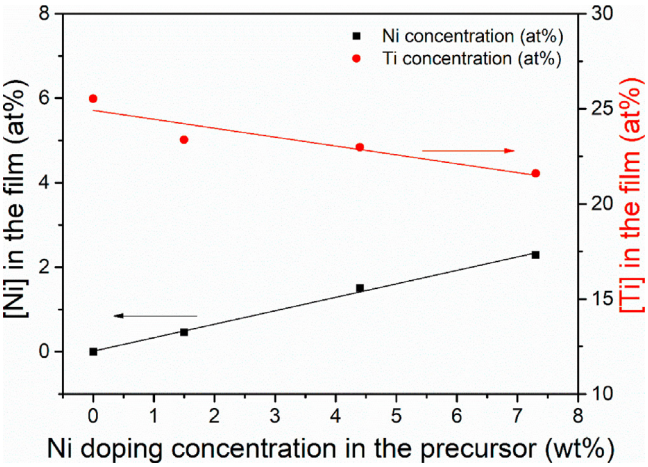

Fig. 6. Variations of the Ni and Ti contents in Ni-doped CCTO films with different concentrations of Ni in the precursor solutions.

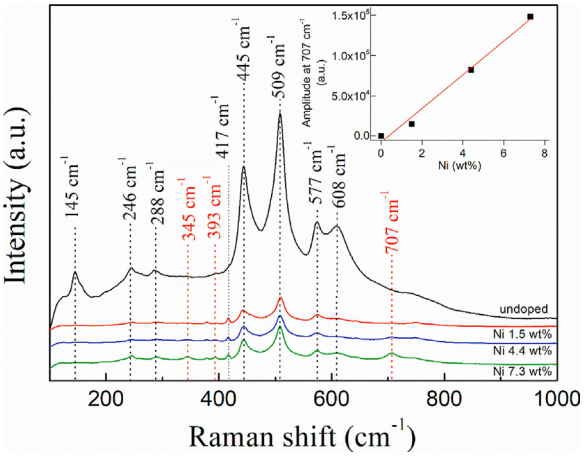

Fig. 7. Raman spectra of pure and Ni-doped CCTO films.

that there is negligible effect of substrate on the crystallization of CCTO films.

The surface morphologies of all films annealed at 800 °C on alumina substrate are shown in Fig. 3. A porous granular form is the common feature among all the films. The 1.5 wt% and 4.4 wt% Ni-doped CCTO films show some clustered forms of granules as seen in Fig. 3(b–c) due possibly to cracking of the film prior to the growth of subsequent layers. The average granule size was estimated to be approximately 65 nm. In addition, the film porosity appears to increase with increasing Ni concentration. The pores in the films could provide additional surface area for efficient interaction with gases. Fig. 4 shows a typical cross sectional image of 7.3 wt% Ni-doped CCTO film on an alumina substrate, demonstrating a film thickness of approximately 470 nm for a four-layer deposition. Some of the porous structures of the films are visible and some voids are deep enough to cross the CCTO film all the way down to the substrate.

To gain access into the chemical composition of the sensing films, EDX spectra were collected on the undoped and 7.3 wt% Ni-doped CCTO films as illustrated in Fig. 5(a) and (b), respectively. The EDX spectra confirmed the presence of calcium (Ca), copper (Cu), titanium (Ti), and oxygen (O) in both films while nickel (Ni) was only detected in the doped film.

The EDX analysis is also useful to identify the lattice site where Ni doping takes place. Fig. 6 shows the plot of measured Ni doping concentrations observed in the film together with the detected Ti concentrations as a function of the Ni doping level used in the sol-gel precursor solutions. It can be seen that the measured Ni atomic percentage in the films increases while the Ti atomic percentage decreases with increasing Ni concentration in the precursor solutions. The correlation between the concentrations of Ni and Ti in the films suggests that Ti atoms was replaced by Ni atoms upon nickel doping. The substitution at Ti sites can feasibly occur without a significant distortion of the lattice since the atomic radius of Ni (149 pm) is smaller than that of Ti (176 pm). This is consistent with the XRD patterns in Fig. 2, which do not show measurable peak shifts for the CCTO signals upon Ni doping at the levels of 1.5–7.3 wt%.

3.2. Raman and XPS studies

Raman spectroscopy was used to indicate the location and type of the sites occupied by the Ni dopant atoms. The Raman spectra for pure and Ni-doped CCTO films in the range of 100–1000 cm^{-1} are shown in Fig. 7. Normal mode analysis of the $Im\bar{3}$ perovskite like unit cell of $CaCu_3Ti_4O_{12}$ predicted a total eight Raman active phonon modes, namely two *Ag*, two *Eg* and four *Fg* peaks [40]. Lattice dynamic calculations assigned the *Ag*, *Eg* and two of the *Fg* modes to rotation-like rocking motions of the TiO_6 octahedrons, and two additional *Fg* modes corresponding to the breathing-stretching motion of the TiO_6 octahedron and the O-Ti-O antistretching motion, respectively [41]. The expected frequencies for the bands of rotation-like motions are $\nu(Ag_1) = 428$, $\nu(Ag_2) = 512$, $\nu(Eg_1) = 318$, $\nu(Eg_1) = 548$, $\nu(Fg_1) = 280$ and $\nu(Fg_2) = 405\ cm^{-1}$ and those of the antistretching and breathing bands are $\nu(Fg_3) = 574$ and $\nu(Fg_4) = 708\ cm^{-1}$, respectively. With exception of Eg_1, Fg_2 and Fg_4 modes, all the remaining bands appear in the undoped

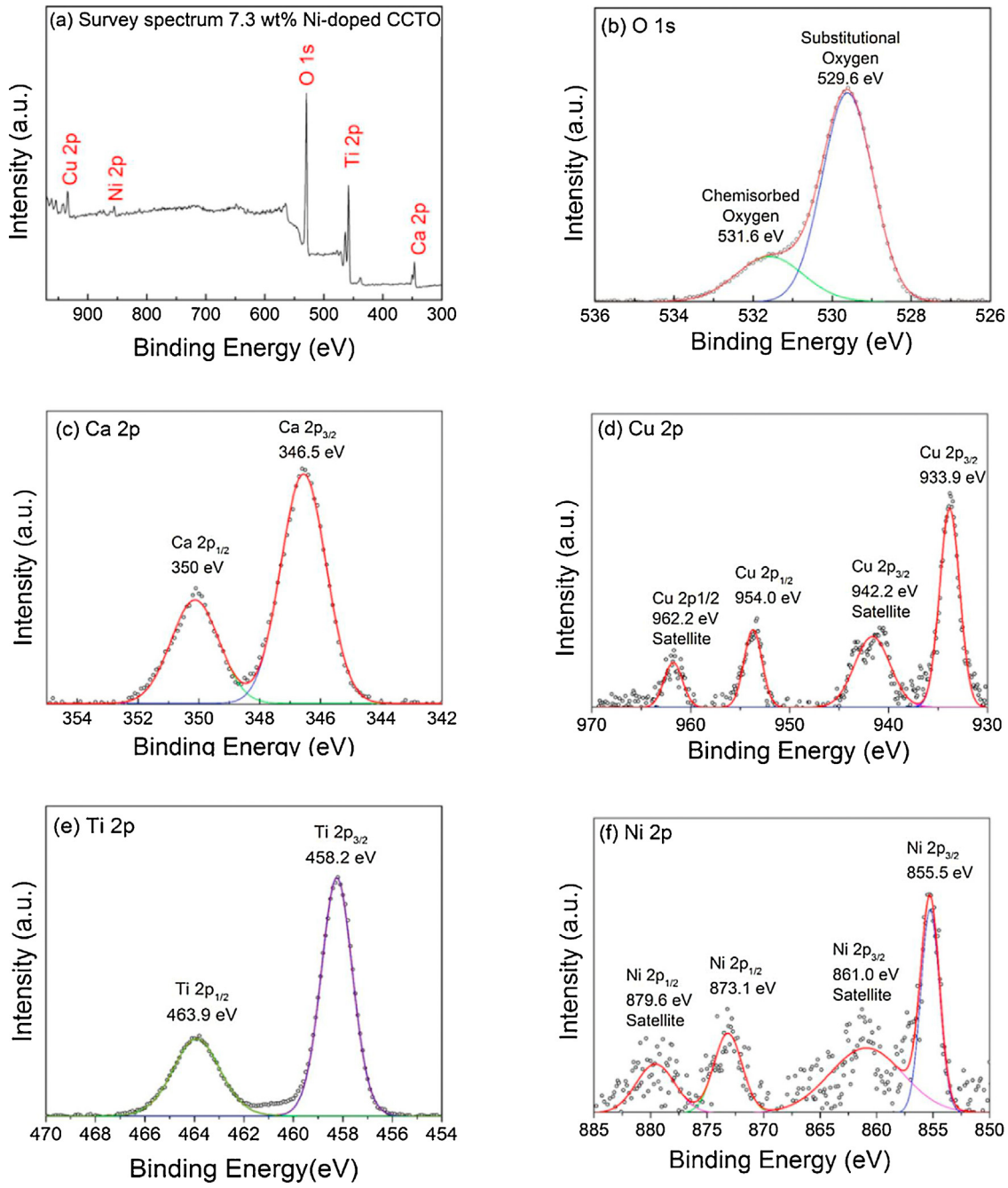

Fig. 8. XPS spectra of (a) survey scan, (b) O 1s, (c) Ca 2p, (d) Cu 2p, (e) Ti 2p, and (f) Ni 2p core levels for 7.3 wt% Ni-doped CCTO film.

CCTO samples near the predicted positions. Further evidence of the hypothesis that Ni doping takes place by substitution at the Ti sites may be found by careful inspection of the Raman spectra. Upon Ni-doping, all the bands show reduced intensities, while the Fg_1 peak is completely absent in agreement with the findings of Li et al. [42]. In the Ni-doped films, new bands at 345, 393, and 707 cm^{-1} labeled in red color in Fig. 7 arise and their intensities tend to increase with increasing Ni concentration. In particular, the intensity of narrow band at 707 cm^{-1} increases linearly with increasing Ni-doping level. In addition, it appears at a similar frequency as that of other substituted perovskites where it was assigned to the symmetric stretching (breathing) mode of the oxygen atoms in close proximity to the substituent [43]. Thus, the 707 cm^{-1} signal is likely to arise from the breathing mode of the NiO_6 octahedral units, further supporting the hypothesis of Ni-Ti substitution upon Ni-doping based on the EDX results in Fig. 6.

In order to characterize the surface chemistry of the Ni-doped CCTO films, X-ray photoelectron (XPS) measurements were carried out. The XPS survey spectrum presented in Fig. 8(a) shows the signatures of O, Ca, Cu, Ti and Ni in the Ni-doped CCTO films. Fig. 8(b) displays the XPS core-level spectrum having two O 1 s peaks located at 529.6 and 531.6 eV, which can be associated with lattice and chemisorbed oxygen species, respectively [17]. The spectrum of the Ca 2p in Fig. 8(c) confirms the 2+ oxidation state of Ca via the $2p_{3/2}$ peak at 346.5 eV [17]. Fig. 8(d) also affirms the presence of copper in 2+ oxidation state from the binding energy values of the $2p_{1/2}$ and $2p_{3/2}$ levels [44,45]. The two satellite peaks of copper can be also observed at binding energies of 942.2 and 962.2 eV, respectively [46]. The Ti 2p spectrum in Fig. 8(e) displays the Ti $2p_{3/2}$and

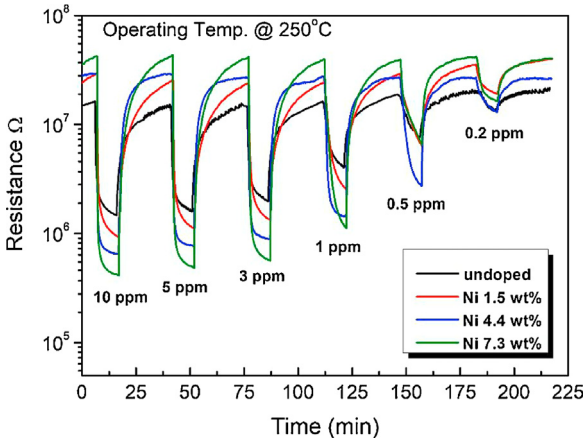

Fig. 9. Resistance changes of undoped CCTO and Ni-doped CCTO subjected to various H_2S pulses at 250 °C.

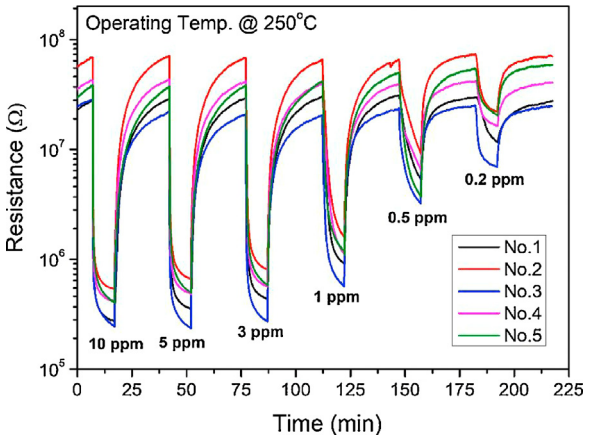

Fig. 10. Resistance changes for five 7.3 wt% Ni-doped CCTO samples fabricated in the same batch subjected to various H_2S pulses at 250 °C.

$2p_{1/2}$ peaks at 458.2 eV and 463.9 eV, which can be assigned to the Ti^{4+} oxidation state [47].

Regarding the oxidation state of the Ni substituent, a hypothetical Ni^{4+} state would show a strong $2p_{3/2}$ signal at 859–861 eV while Ni^{3+} and Ni^{2+} states should exhibit $2p_{3/2}$ signals at 856.0 eV and 854.5 eV, respectively [48]. From the XPS data of Ni 2p core level presented in Fig. 8(f), the Ni $2p_{1/2}$ and $2p_{3/2}$ peaks are located at 873.1 eV and 855.5 eV, respectively. Thus, they are corresponding to the Ni^{2+} oxidation state [49–51]. The satellite peaks seen at binding energies of 879.6 and 861.0 eV for Ni $2p_{1/2}$ and Ni $2p_{3/2}$, respectively, are also close to the observed binding energies of the Ni^{2+} oxidation state in metal oxides. Therefore, it can be concluded based on the experimental evidences that the Ni^{2+} ions substitute the Ti^{4+} ions at the octahedral TiO_6 lattice site.

3.3. Characterization of the gas sensing devices

Fig. 9 shows the resistance curves of Ni-doped CCTO sensors subjected to various H_2S concentrations in the range of 0.2–10 ppm at 250 °C. When the sensors are in air atmosphere, they have the resistance values on the order of 10^7 ohms. Upon introduction of H_2S gas, the resistance suddenly decreases by an amount that depends on the H_2S concentration. The results are consistent with an n-type semiconductor character towards a reducing gas, in agreement with previous works [11,52]. Returning the sensors to an air atmosphere restores the initially high resistance state and repeated cycling between streams of air with and without the target gas demonstrates good sensor response and repeatable baseline recovery over several hours of sensing tests. In addition, it can be observed that the magnitude of resistance change tends to increase with increasing Ni doping level up to 7.3 wt%. Fig. 10 illustrates the resistance variation of five 7.3 wt% Ni-doped CCTO sensors fabricated from the same batch. It is seen that the Ni-doped CCTO sensing films prepared by the sol-gel method exhibit good reproducibility of resistance response with the variation of baseline resistance of less than 40%. In addition, it displays reproducible change of resistances at each gas concentration with the total deviation of less than 30%. The attained reproducibilty of the sensing films is superior to random nanostructured sensors and can be attributed to the reproducibility of the thin film fabrication process based on the sol-gel and spin-coating methods.

The operating temperature of a metal oxide semiconductor gas sensor has marked effects on its performances due to the complex interplay of gas-surface interactions. From a practical point of view, a sensing device should operate optimally at the lower working temperature in order to reduce the power consumption. Fig. 11(a)

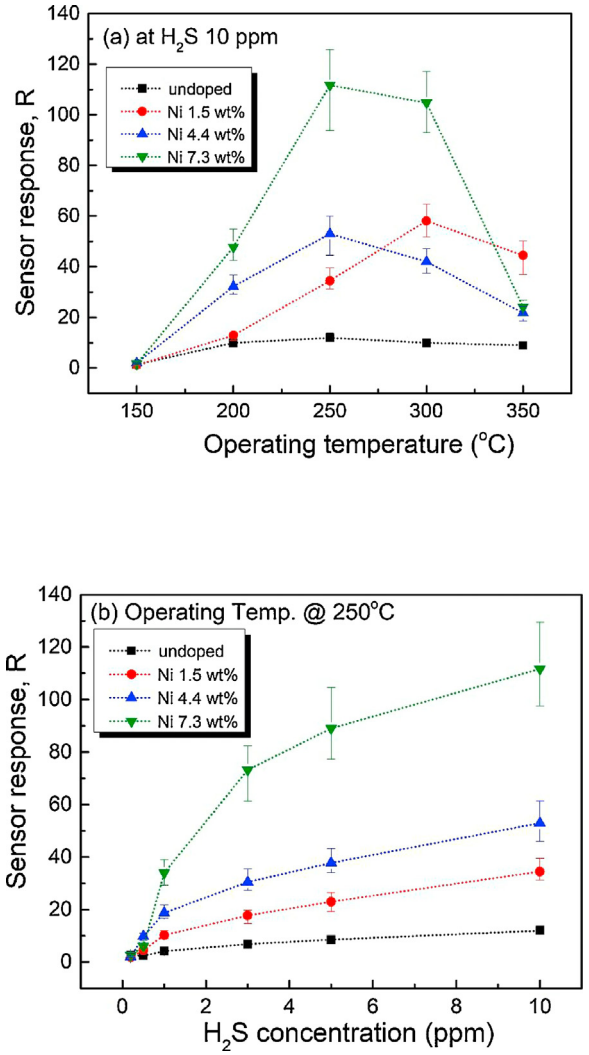

Fig. 11. Response of undoped CCTO and Ni-doped CCTO (a) as a function of operating temperatures ranging from 150 to 350 °C to 10 ppm H_2S and (b) as a function of H_2S concentration at the optimal working temperature of 250 °C.

shows the sensor response ($R = R_a/R_g$) as a function of operating temperature in the range of 150–350 °C. As the operating temperature increases, the H_2S response of all films initially increases and then reaches a maximum value at an optimal working temperature

before decreasing at higher temperatures. This behavior indicates that the response is restricted by the speed of chemical reaction at low temperatures and limited by the speed of diffusion of H_2S to and from the sensor surface at high temperatures [5]. At a moderate temperature, the speed of chemical reaction and diffusion are balanced resulting in the maximum response for a given target gas [5]. From the results, Ni-doping causes two marked effects on the temperature response curve of CCTO films including the increase of the maximum response value and the lower optimal working temperature from 300 to 250 °C with increasing Ni content from 1.5 to 4.4 and 7.3 wt%. The best sensor response to 10 ppm H_2S of 112 is obtained with the 7.3 wt% Ni content at 250 °C. The sensor response as function of the H_2S concentrations at the optimum operating temperature of 250 °C are presented in Fig. 11(b). It is seen that the sensor response of all the films increases monotonically with increasing H_2S concentrations but the increment tends to be less at high gas concentrations of 3–10 ppm. The behavior conforms to the well-known power law with the exponent values of less than 1 [11,12]. Also, the response at a given H_2S concentration increases with increasing Ni doping level. Moreover, all error bars in Fig. 11 representing the response variation of five sensors made from the same batch demonstrate that sensors exhibit good reproducibility with the response deviation of less than 30% under all tested conditions.

To characterize the response speed of the CCTO films, the response and recovery times were calculated and analyzed. The response time for the gas sensors is taken to be the time elapsed while the electrical resistance of the sensor varies between the 10% and 90% of the steady-state resistance upon sudden exposure to the stream containing H_2S gas. Similarly, the recovery time is measured from the 90% to 10% of stable resistance upon sudden switching from the H_2S-containing stream to pure dry air [53]. Fig. 12(a,b) show the response and recovery times of our Ni-doped CCTO sensors as a function of H_2S concentration varying from 0.2 to 10 ppm.

It can be seen that the response and recovery times are the longest for undoped CCTO and tend to decrease with increasing nickel doping level especially at the sub-ppm concentrations of H_2S. When the sensors operate at higher H_2S concentrations, the response time decreases while the recovery time increases slowly with increasing H_2S concentration. The shortest response times are thus obtained at the highest H_2S concentration of 10 ppm. The shortest response time of undoped CCTO sensor is 58 s while those of 1.5, 4.4 and 7.3 wt% Ni-doped films are considerably lower at 20, 7 and 5 s, respectively. In addition, the 4.4 wt% and 7.3 wt% Ni-doped CCTO films exhibit the shortest response and recovery times at any H_2S concentrations. The shorter response time can be attributed to faster occupation of active surface sites for H_2S binding at higher H_2S concentration while the longer recovery time is due to the need to remove the larger amount of the excess charge carriers deposited in the film via the reactions with H_2S.

To be of practical use, a gas sensor should provide a strong specific response to a single target gas. Thus, the relative response of undoped and Ni-doped CCTO gas sensing devices were measured towards different gases including H_2S, H_2, NH_3, NO_2 and ethanol at the optimal working temperature of 250 °C as displayed in Fig. 13. Since the responses to H_2, NH_3 and ethanol were very low, these gases were introduced at much higher concentrations compared with 10 ppm of H_2S and 5 ppm of NO_2. It is evident that the response to H_2S is vastly improved (ca. 10 times) and the response to NO_2 is slightly improved (ca. 3 times) while the responses to other gases are not significantly increased as the Ni-doping level increases from 0 to 7.3 wt%. Thus, the Ni-doped CCTO sensors are highly selective towards H_2S with a relative response at least an order of magnitude higher than other tested gases and they are highly potential for selective detection of H_2S.

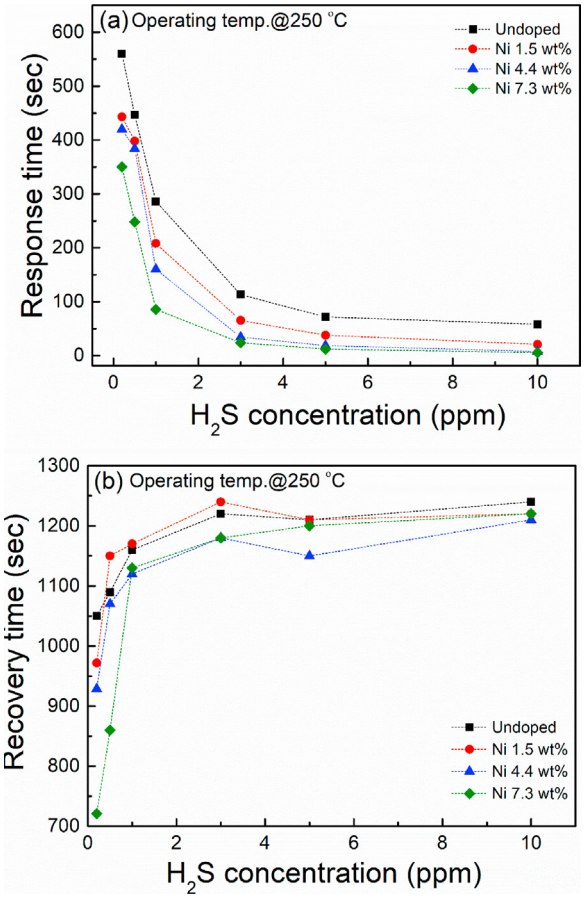

Fig. 12. (a) Response and (b) recovery times of undoped and Ni-doped CCTO sensors to different H_2S concentrations (from 0.2 to 10 ppm).

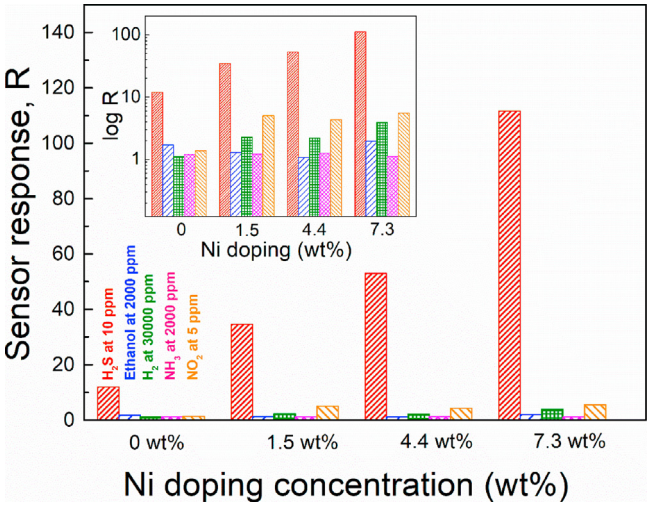

Fig. 13. Selectivity histograms exhibited by the undoped CCTO and Ni-doped CCTO sensors towards various gases at 250 °C. The insert emphasizes the lowest responses in logarithmic scale.

3.4. Gas sensing mechanism

The general working principle of metal oxide semiconductor gas sensors is based on the modulation of the electrical conductivity caused by interactions of the metal oxide sensing surface with the carrier and target gases. A myriad of chemical reactions occurs concurrently with diffusion processes which make the full

understanding of the gas sensor a challenge. Therefore, an empirical model is usually invoked to explain the fundamental gas sensing mechanism. Within this model, a sensor is initially under an oxidizing air atmosphere. At the operating temperature, molecular oxygen is chemisorbed from the gas phase onto the metal oxide surface where it creates extrinsic surface acceptor states that capture conduction band electrons near the surface zone of metal oxide, forming $O^-_{2\ adsorbed}$ species [5,11,31,54], which will further interact with electrons via the reaction,

$$O^-_{2\ adsorbed} + 2e^-_{surf} \rightleftarrows 2O^-_{adsorbed} \quad (1)$$

In addition, molecular oxygen will diffuse into the lattice of the metal oxide until encountering an oxygen vacancy defect at the crystal. At this point, an oxygen ion fills the vacancy and causes the immobilization of an additional pair of conduction electrons via

$$\frac{1}{2}O^{gas}_2 + V^{\bullet\bullet}_O + 2e^- \rightleftarrows O^{2-}_{lattice} \quad (2)$$

where $V^{\bullet\bullet}_O$ denotes an oxygen vacancy. In the case of the n-type semiconducting CCTO, the oxygen immobilization processes create a depletion layer at the skin region near surfaces of the sensor material, resulting in the lowering of the Fermi level. Introducing gases with reducing properties will consequently counteract this depletion layer, replenishing the density of charge carriers in the near-surface region of CCTO and raising the Fermi level. In contrast, an oxidizing gas would further decrease the charge carrier density, widen the depletion layer and lower the Fermi level. Charge depletion induced by oxygen and other oxidizing gas species therefore increases the resistivity of an n-type metal oxide while the reducing gases would counterbalance the charge depletion and reduce the metal oxide resistivity. From the chemical point of view, the compensation of charge depletion occurs via the oxidation of the target gas. Following adsorption of H_2S, the possible surface oxidation reactions include [27,34,35]:

$$2H_2S_{adsorbed} + 3O^-_{2adsorbed} \xrightarrow{k_1} 2SO_2 + H_2O + 3e^- \quad (3)$$

$$H_2S_{adsorbed} + 3O^{2-}_{adsorbed} \xrightarrow{k_2} SO_2 + H_2O + 6e^- \quad (4)$$

$$5O^x_{lattice} + H_2S_{adsorbed} \xrightarrow{k_3} SO^{2-}_4 + H_2O + 3V^{\bullet\bullet}_O + 6e^- \quad (5)$$

Each of these reactions is likely to involve several elementary stages such as diffusion to a particular specific site where one or more electrons are transferred as well as surface mobilization of adsorbed oxygen and H_2S species to a particular highly reactive lattice site. The higher sensor response in Ni-doped CCTO sensors relative to undoped ones suggest that Ni ions are directly responsible for facilitating some of the steps in Eqs. (3)–(5). In the present work, the choice of Ni as a doping element was based on the well-established strong interaction of Ni-catalysts with sulfur compounds causing a poisoning effect [34,35]. Indeed Eqs. (3) and (4) correspond to the catalyst regeneration to counteract the sulfur poisoning. We propose the hypothesis that the specific sites at which the H_2S molecules adsorb and react with the Ni-doped CCTO films are the surface sites where Ni^{2+} ions are exposed. In order to examine the role of the Ni^{2+} ions on the H_2S sensor response, the reciprocal of the sensor response time (response rate) is analyzed as a function of the Ni-doping concentration in CCTO. This analysis can reveal the catalytic effects of the Ni-doping since what ultimately governs the drop of the sensor resistivity upon H_2S exposure is the rate at which electrons are transferred from the reacting H_2S species into the charge depletion zone.

Fig. 14 shows that the response rates are approximately linear functions of the H_2S gas concentration at all Ni-doping levels, which suggests that a first order kinetics of H_2S interaction dominates the 10/90% portion of the sensing response. This representation

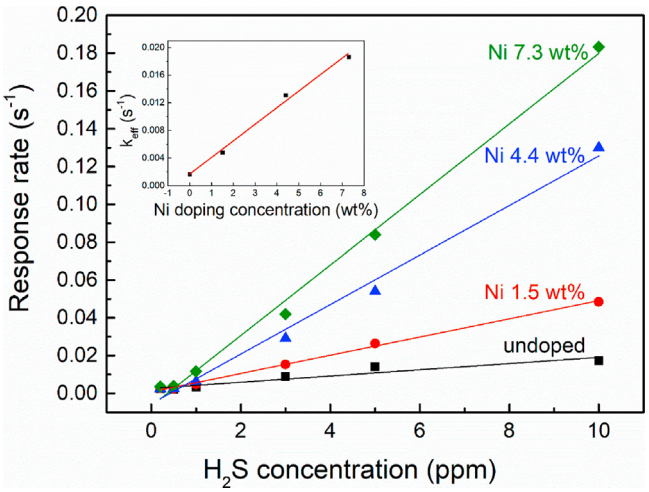

Fig. 14. Dependence of the sensor response rate on H_2S concentration. Inset: the specific response rate versus the nickel doping concentration (black squares) and linear fit (red solid line). (For interpretation of the references to colour in this figure legend, the reader is referred to the web version of this article.)

allows the identification of a specific response rate dependence on the Ni-doping level. The slopes of the linear functions in Fig. 14 are referred to as the effective response rates (k_{eff}). A plot of k_{eff} versus the Ni-doping concentration allows us to estimate the reaction order in the catalyst as shown in the inset on Fig. 14. The observed linear dependence on the Ni-doping is the indicative of a first order catalytic effect. In the light of the reactions stated in Eqs. (3)–(5), a possible mechanistic explanation for these results is represented in Fig. 15. The first step represents the sensor in the standby situation with chemisorbed oxygen species on surface under air atmosphere. Upon introducing H_2S gas, steps 2–5 take place. In step 2, H_2S molecules adsorb on the Ni-doped CCTO surface at sites where Ni^{2+} ion is present, possibly by substitution of one of the oxygen ligands and forming a sulfide ion plus a water molecule. Subsequently (steps 3–5), the six-electron oxidation of a single H_2S molecule necessarily occurs sequentially to convert from S^{2-} by passing through S^0 all the way to S^{4+} before desorption of the final product of SO_2 gas. In the process, the formation of elementary sulfur (S^0) from H_2S is more likely to become the rate limiting process since the oxidation of S^0 into SO_2 is a very exothermic process. At this rate-limiting step, two electrons are transferred from the sulfide ion to the Ni^{2+} ion to form a reduced Ni^0 state and produce an adsorbed sulfur atom. Finally, electrons will be injected from S^0 into the conduction band to restore the Ni^{2+} state while the elemental sulfur atoms are oxidized into SO_2 gas.

The electrons transferred to the conduction band of the CCTO neutralizes the depletion charges initially induced by reactions in Eqs. (1)–(2) and raises the Fermi level of the material, resulting in higher conductivity of the gas sensor. Being a relatively noble metal, Ni supports the +2 and 0 oxidation states that can interconvert relatively easily, thus facilitating the 2-electron oxidation of H_2S as well as the recovery to the +2 state when the sensor returns to the standby condition in air. The small response of undoped CCTO towards H_2S is likely due to a distinct role played by copper. A hint to a plausible explanation of the higher H_2S-sensing response of nickel may be based on the free energies for formation of the oxides and sulfides of copper and nickel. On one hand, copper has more tendency to become oxidized because the formation of CuO is more exergonic ($\Delta G^0_f = -372$ kJ/mole) than that of NiO ($\Delta G^0_f = -213$ kJ/mole). On the other hand, nickel sulfide (NiS) is more stable than copper sulfide (CuS) ($\Delta G^0_{f(NiS)} = -90$ kJ/mole and $\Delta G^0_{f(CuS)} = -49$ kJ/mole). Therefore, Ni-doping improves the

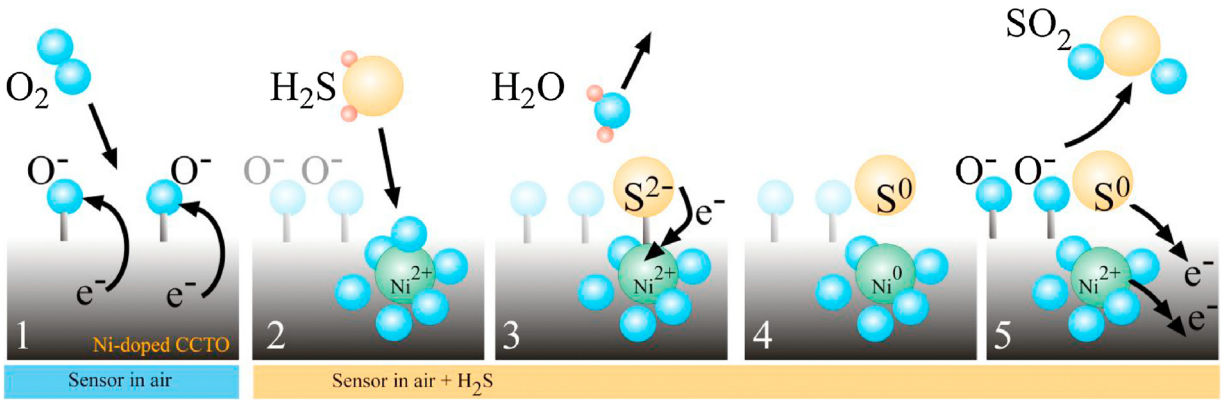

Fig. 15. Schematic representation of the proposed H_2S-sensing mechanism of the Ni-doped CCTO gas sensor.

H_2S response of CCTO films by facilitating the sulfur binding and subsequent oxidation of sulfide species.

4. Conclusions

Ni-doped CCTO films can be used as the active medium for the fabrication of specific H_2S gas sensors with decent H_2S responses in the concentration range of 0.2–10 ppm. The sensor response depends on the doping level, reaching 120 at the Ni doping level of 7.3 wt%. The Ni-doped CCTO film sensors operating optimally at 250 °C are 10 times more sensitive to H_2S than to NO_2 and over 2 orders of magnitude more sensitive to H_2S than to H_2, NH_3, and ethanol vapor. Ni ions play a catalytic role in the oxidation of adsorbed sulfur species enhancing the response of the sensors. Therefore, the sol-gel Ni-doped CCTO films offer particularly attractive sensing features including high selectivity towards H_2S, decent sensitivity for detection of sub ppm concentrations of H_2S and good reproducibility.

Acknowledgments

Authors would like to thank the 90th Anniversary of Chulalongkorn University Fund to support budgets for this research. Dr. Satreerat K. Hodak thanks the Thailand Research Fund (TRF) for grant RSA6080016. Dr. Jose Hector Hodak would like to thank Chulalongkorn University for providing a visiting professor grant. We would like to thank MINCYT for grant PICT-2012-2041 and UBA for grant UBACYT 01/Q643. We would like to specially thank to Dr. Adisorn Tuantranont and National Electronics and Computer Technology (NECTEC) for gas-sensing facilities. This research was partially supported by Ratchadapiseksomophot Endowment under Outstanding Research Performance Program (SciSuper III).

References

[1] I.P.o.C.S.a.W.H. Organisation, Concise International Chemical Assessment, Document 53 - Hydrogen Sulphide: Human Health Aspects, World Health Organization, Geneva, Switzerland, 2003.
[2] M.F. Struve, J.N. Brisbois, R. Arden James, M.W. Marshall, D.C. Dorman, Neurotoxicological effects associated with short-Term exposure of Sprague–Dawley rats to hydrogen sulfide, Neurotoxicology 22 (2001) 375–385.
[3] T.W. Lambert, V.M. Goodwin, D. Stefani, L. Strosher, Hydrogen sulfide (H_2S) and sour gas effects on the eye. A historical perspective, Sci. Total Environ. 367 (2006) 1–22.
[4] R.J. Lewis, G.B. Copley, Chronic low-level hydrogen sulfide exposure and potential effects on human health: a review of the epidemiological evidence, Crit. Rev. Toxicol. 45 (2015) 93–123.
[5] Y. Wang, F. Qu, J. Liu, Y. Wang, J. Zhou, S. Ruan, Enhanced H_2S sensing characteristics of CuO-NiO core-shell microspheres sensors, Sens. Actuators B Chem. 209 (2015) 515–523.
[6] S.L. Darshane, S.S. Suryavanshi, I.S. Mulla, Nanostructured nickel ferrite: a liquid petroleum gas sensor, Ceram. Int. 35 (2009) 1793–1797.
[7] L. Mai, L. Xu, Q. Gao, C. Han, B. Hu, Y. Pi, Single (-$AgVO_3$ nanowire H2S sensor, Nano Lett. 10 (2010) 2604–2708.
[8] N. Minh Vuong, D. Kim, H. Kim, Porous Au-embedded WO_3 nanowire structure for efficient detection of CH_4 and H_2S, Sci. Rep. 5 (2015) 11040.
[9] X. Kong, Y. Li, High sensitivity of CuO modified SnO_2 nanoribbons to H_2S at room temperature, Sens. Actuators B 105 (2005) 449–453.
[10] V.V. Sysoev, B.K. Button, K. Wepsiec, S. Dmitriev, A. Kolmakov, Toward the nanoscopic electronic nose: hydrogen vs carbon monoxide discrimination with an array of individual metal oxide nano- and mesowire sensors, Nano Lett. 6 (2006) 1584–1588.
[11] K. Govardhan, A.N. Grace, Metal/Metal oxide doped semiconductor based metal oxide gas sensors: a review, Sens. Lett. 14 (2016) 741–750.
[12] S.M. Kanan, O.M. El-Kadri, I.A. Abu-Yousef, M.C. Kanan, Semiconducting metal oxide based sensors for selective gas pollutant detection, Sens. (Basel, Switzerland) 9 (2009) 8158–8196.
[13] Z. Lin, W. Song, H. Yang, Highly sensitive gas sensor based on coral-like SnO_2 prepared with hydrothermal treatment, Sens. Actuators B Chem. 173 (2012) 22–27.
[14] J.P. Cheng, J. Wang, Q.Q. Li, H.G. Liu, Y. Li, A review of recent developments in tin dioxide composites for gas sensing application, J. Ind. Eng. Chem. 44 (2016) 1–22.
[15] W. Yu-De, C. Zhan-Xian, L. Yan-Feng, Z. Zhen-Lai, W. Xing-Hui, Electrical and gas-sensing properties of WO_3 semiconductor material, Solid-State Electron. 45 (2001) 639–644.
[16] V. Galstyan, E. Comini, C. Baratto, G. Faglia, G. Sberveglieri, Nanostructured ZnO chemical gas sensors, Ceram. Int. 41 (2015) 14239–14244.
[17] P.R. Bueno, R. Tararan, R. Parra, E. Joanni, M.A. Ramírez, W.C. Ribeiro, et al., A polaronic stacking fault defect model for $CaCu_3Ti_4O_{12}$ material: an approach for the origin of the huge dielectric constant and semiconducting coexistent features, J. Phys. D: Appl. Phys. 42 (2009) 055404.
[18] R. Jiménez, M.L. Calzada, I. Bretos, J.C. Goes, A.S.B. Sombra, Dielectric properties of sol-gel derived $CaCu_3Ti_4O_{12}$ thin films onto $Pt/TiO_2/Si(100)$ substrates, J. Eur. Ceram. Soc. 27 (2007) 3829–3833.
[19] Y.L. Zhao, G.W. Pan, Q.B. Ren, Y.G. Cao, L.X. Feng, Z.K. Jiao, High dielectric constant in $CaCu_3Ti_4O_{12}$ thin film prepared by pulsed laser deposition, Thin Solid Films 445 (2003) 7–13.
[20] P. Mishra, P. Kumar, Structural, dielectric and optical properties of [(BZT–BCT)-(epoxy-CCTO)] composites, Ceram. Int. 41 (2015) 2727–2734.
[21] W.-X. Yuan, S.K. Hark, H.Y. Xu, W.N. Mei, Investigation on the growth of $CaCu_3Ti_4O_{12}$ thin film and the origins of its dielectric relaxations, Solid State Sci. 14 (2012) 35–39.
[22] R.L. Nigro, R.G. Toro, G. Malandrino, I.L. Fragalà, P. Fiorenza, V. Raineri, Effects of high temperature annealing on MOCVD grown $CaCu_3Ti_4O_{12}$ films on $LaAlO_3$ substrates, Surf. Coat. Technol. 201 (2007) 9243–9247.
[23] K.D. Mandal, A.K. Rai, D. Kumar, O. Parkash, Dielectric properties of the $Ca_{1-x}La_xCu_3Ti_{4-x}Co_xO_{12}$ system (x = 0. 10, 0. 20 and 0. 30) synthesized by semi-wet route, J. Alloys Compd. 478 (2009) 771–776.
[24] Z. Yang, Y. Zhang, G. You, K. Zhang, R. Xiong, J. Shi, Dielectric and electrical transport properties of the Fe^{3+}-doped $CaCu_3Ti_4O_{12}$, J. Mater. Sci. Technol. 28 (2012) 1145–1150.
[25] J.-W. Lee, J.-H. Koh, Enhanced dielectric properties of Ag-doped CCTO ceramics for energy storage devices, Ceram. Int. 43 (2017) 9493–9497.
[26] C. -h. Zhang, K. Zhang, H. -x. Xu, Q. Song, Y. -t. Yang, R. -h. Yu, et al., Microstructure and electrical properties of sol–gel derived Ni-doped $CaCu_3Ti_4O_{12}$ ceramics, Trans. Nonferrous Met. Soc. China 22 (2012) s127–s132.
[27] S. Pongpaiboonkul, D. Phokharatkul, J.H. Hodak, A. Wisitsoraat, S.K. Hodak, Enhancement of H2S-sensing performances with Fe-doping in $CaCu_3Ti_4O_{12}$ thin films prepared by a sol–gel method, Sens. Actuators B Chem. 224 (2016) 118–127.

[28] X. Wang, M. Zhao, F. Liu, J. Jia, X. Li, L. Cao, C_2H_2 gas sensor based on Ni-doped ZnO electrospun nanofibers, Ceram. Int. 39 (2013) 2883–2887.
[29] H. Gong, J.Q. Hu, J.H. Wang, C.H. Ong, F.R. Zhu, Nano-crystalline Cu-doped ZnO thin film gas sensor for CO, Sens. Actuators B Chem. 115 (2006) 247–251.
[30] J.-C. Ding, H.-Y. Li, T.-C. Cao, Z.-X. Cai, X.-X. Wang, X. Guo, Characteristics and sensing properties of CO gas sensors based on $LaCo_{1-x}Fe_xO_3$ nanoparticles, Solid State Ionics 303 (2017) 97–102.
[31] Z. Lin, N. Li, Z. Chen, P. Fu, The effect of Ni doping concentration on the gas sensing properties of Ni doped SnO_2, Sens. Actuators B Chem. 239 (2017) 501–510.
[32] W.-T. Li, X.-D. Zhang, X. Guo, Electrospun Ni-doped SnO_2 nanofiber array for selective sensing of NO2, Sens. Actuators B Chem. 244 (2017) 509–521.
[33] H. Zhongqiu, Y. Masayoshi, K. Tetsuya, Y. Noboru, S. Kengo, H2 sensing mechanism of Pd-Loaded WO_3 nanoparticle gas sensors, Chem. Lett. 43 (2014) 1435–1437.
[34] W.A. Wan Abu Bakar, M.Y. Othman, R. Ali, C.K. Yong, Nickel oxide based supported catalysts for the In-situ reactions of methanation and desulfurization in the removal of sour gases from simulated natural gas, Catal. Lett. 128 (2009) 127–136.
[35] D.K. Niakolas, Sulfur poisoning of Ni-based anodes for solid oxide fuel cells in H/C-based fuels, Appl. Catal. A: Gen. 486 (2014) 123–142.
[36] C. Balamurugan, Y.J. Jeong, D.W. Lee, Enhanced H_2S sensing performance of a p-type semiconducting pdO-NiO nanoscale heteromixture, Appl. Surf. Sci. 420 (2017) 638–650.
[37] X. Liu, J. Zhang, X. Guo, S. Wu, S. Wang, Enhanced sensor response of Ni-doped SnO_2 hollow spheres, Sens. Actuators B Chem. 152 (2011) 162–167.
[38] H.-M. Huang, H.-Y. Li, X.-X. Wang, X. Guo, Detecting low concentration of H_2S gas by $BaTiO_3$ nanoparticle-based sensors, Sens. Actuators B Chem. 238 (2017) 16–23.
[39] S. Yuvaraj, V.D. Nithya, K.S. Fathima, C. Sanjeeviraja, G.K. Selvan, S. Arumugam, et al., Investigations on the temperature dependent electrical and magnetic properties of $NiTiO_3$ by molten salt synthesis, Mater. Res. Bull. 48 (2013) 1110–1116.
[40] D.L. Rousseau, R.P. Bauman, S.P.S. Porto, Normal mode determination in crystals, J. Raman Spectrosc. 10 (1981) 253–290.
[41] N. Kolev, R.P. Bontchev, A.J. Jacobson, V.N. Popov, V.G. Hadjiev, A.P. Litvinchuk, et al., Raman spectroscopy of $CaCu_3Ti4O_{12}$, Phys. Rev. B 66 (2002) 132102.
[42] T. Li, J. Chen, D. Liu, Z. Zhang, Z. Chen, Z. Li, et al., Effect of NiO-doping on the microstructure and the dielectric properties of $CaCu_3Ti_4O_{12}$ ceramics, Ceram. Int. 40 (2014) 9061–9067.
[43] A. Dubroka, J. Humlíček, M.V. Abrashev, Z.V. Popović, F. Sapiña, A. Cantarero, Raman and infrared studies of $La_{1-y}Sr_yMn_{1-x}M_xO_3$ (M = Cr, Co, Cu, Zn, Sc or Ga): Oxygen disorder and local vibrational modes, Phys. Rev. B 73 (2006) 224401.
[44] J.F. Fernández, P. Leret, J.J. Romero, J. de Frutos, M.Á. de la Rubia, M.S. Martín-González, et al., Proofs of the coexistence of two magnetic contributions in pure and doped $CaCu_3Ti_4O_{12}$ giant dielectric constant ceramics, J. Am. Ceram. Soc. 92 (2009) 2311–2318.
[45] M. Xue, Y. Tan, Hollow alloy nanostructures templated by Au nanorods: synthesis, mechanistic insights, and electrocatalytic activity, Nanoscale 6 (2014) 12500–12514.
[46] M. Kuang, T.T. Li, H. Chen, S.M. Zhang, L.L. Zhang, Y.X. Zhang, Hierarchical $Cu_2O/CuO/Co_3O_4$ core-shell nanowires: synthesis and electrochemical properties, Nanotechnology 26 (2015) 304002.
[47] W. Hao, H. Wu, P. Xu, Y. Shi, S. Yang, M. Wang, et al., Influence of Sb-doping on dielectric properties of $NaCu_3Ti_3TaO_{12}$ ceramics and relevant mechanism(s), Ceram. Int. 43 (2017) 3631–3638.
[48] R. Gottschall, R. Schöllhorn, M. Muhler, N. Jansen, D. Walcher, P. Gütlich, Electronic state of nickel in barium nickel oxide, $BaNiO_3$, Inorg. Chem. 37 (1998) 1513–1528.
[49] L. Rambu, N. Ursu, V. Iftimie, M. Nica, F. Dobromir, Study on Ni-doped ZnO films as gas sensors, Appl. Surf. Sci. 280 (2013) 598–604.
[50] S. Mickevičius, S. Grebinskij, V. Bondarenka, B. Vengalis, K. Šliužienė, B.A. Orlowski, et al., Investigation of epitaxial $LaNiO_{3-x}$ thin films by high-energy XPS, J. Alloys Compd. 423 (2006) 107–111.
[51] S. Luisetto, C. Tuti, S. Lo Mastro, A. Sodo, Ni/CeO_2–Al_2O_3 catalysts for the dry reforming of methane: the effect of $CeAlO_3$ content and nickel crystallite size on catalytic activity and coke resistance, Appl. Catal. A: Gen. 500 (2015) 12–22.
[52] D. Varshney, A. Kumar, Structural and optical properties of Ni substituted $CaCu_3Ti_{4-x}Ni_xO_{12}$, Opt. Int. J. Light Electron. Opt. 126 (2015) 3437–3441.
[53] J.P. Blanc, N. Derouiche, A. El Hadri, J.P. Germain, C. Maleysson, H. Robert, Study of the action of gases on a polypyrrole film, Sens. Actuators B Chem. 1 (1990) 130–133.
[54] L. Huo, X. Yang, Z. Liu, X. Tian, T. Qi, X. Wang, et al., Modulation of potential barrier heights in Co_3O_4/SnO_2 heterojunctions for highly H_2-selective sensors, Sens. Actuators B Chem. 244 (2017) 694–700.

Biographies

Arisara Boontum was born in Surin, Thailand. She received the Science Achievement Scholarship of Thailand (SAST) in 2010–2015. She finished Bachelor degree in Physics, Department of Physics, Faculty of Science, Ubon Ratchathani University, in 2013. She is currently studying for her M.Sc. degree in Physics, Department of Physics, Faculty of Science, Chulalongkorn University. Her research interests include the synthesis of Ni-doped calcium copper titanate thin films and their gas sensing properties.

Ditsayut Phokharatkul is an assistant researcher at MEMS Laboratory in NECTEC, Thailand. He received his B.E. and M.E. degrees from Nagoya University (Japan) in 2006 and 2008, respectively. His dissertation is development of high density horizontally aligned carbon nanotubes for CNT-FET application. His research interests include microelectronic fabrication, semiconductor devices, carbon nanotubes, graphene and sensors.

Anurat Wisitsoraat received his Ph.D., M.S. degrees from Vanderbilt University, TN, U.S.A., and B. Eng degree in electrical engineering from Chulalongkorn University, Bangkok, Thailand in 2002, 1997, and 1993, respectively. His research interests include microelectronic fabrication, semiconductor devices, electronic and optical thin film coating, sensors, and micro electromechanical systems (MEMS).

Jose Hector Hodak was born in Buenos Aires, Argentina. He obtained his Ph.D. in Physical Chemistry at University of Notre Dame, Indiana, USA, in 2001 studying the ultra-fast dynamics of metal nanoparticles. Dr. Hodak worked from 2001 to 2004 as a postdoctoral researcher at JILA-University of Colorado, where he carried out single molecule fluorescence experiments in RNA. He worked as a researcher at the Department of Physics, Mahidol University, Thailand from 2005 until 2010. He is currently an independent investigator of CONICET and assistant professor at the University of Buenos Aires. His research interests are single molecule and ultrafast spectroscopies and analytical chemistry. He was also a visiting professor at Chulalongkorn University, Thailand.

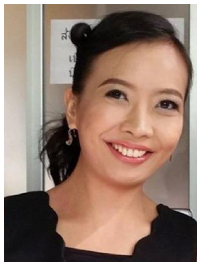

Satreerat Kampangkeaw Hodak was born in Chiang Mai, Thailand. She received her M.Sc in 2000 and her Ph.D. in 2004 from the Department of Physics at University of Colorado, at Boulder, USA studying strontium titanate thin films grown by pulsed laser deposition. She worked as a lecturer from 2005 to 2008 and became an assistant professor from 2008 to 2014. Currently, she is associate professor at the Department of Physics, Chulalongkorn University, Thailand. Her research interests are synthesis and characterization of perovskite oxide thin films and their applications in dielectric, luminescent and gas sensing film devices.